Bioactive Materials 21 (2023) 531–546

Contents lists available at ScienceDirect

Bioactive Materials

journal homepage: www.keaipublishing.com/en/journals/bioactive-materials

Cytokine nanosponges suppressing overactive macrophages and dampening systematic cytokine storm for the treatment of hemophagocytic lymphohistiocytosis

Honglan Wang [a,1], Huiwen Liu [a,1], Jia Li [c], Chunying Liu [b], Hui Chen [d], Junying Li [a], Chunyan Sun [a], Tao Guo [a], Zhiqing Pang [b,*], Bo Zhang [a,**], Yu Hu [a,***]

[a] Institute of Hematology, Union Hospital, Tongji Medical College, Huazhong University of Science & Technology, Wuhan, Hubei, 430022, PR China
[b] School of Pharmacy, Fudan University, Key Laboratory of Smart Drug Delivery, Ministry of Education, 826 Zhangheng Road, Shanghai, 201203, PR China
[c] Department of Biomedical Sciences, Faculty of Medicine, Health and Human Sciences, Macquarie University, Sydney NSW, 2109, Australia
[d] Department of Infectious Diseases, Union Hospital, Tongji Medical College, Huazhong University of Science and Technology, Wuhan, 430022, PR China

ARTICLE INFO

Keywords:
Hemophagocytic lymphohistiocytosis
Cytokine storm
Nanosponge
Macrophage activation
Macrophage membranes coated nanoparticles
Lipopolysaccharide
JAK/STAT pathway

ABSTRACT

Hemophagocytic lymphohistiocytosis (HLH) is a highly fatal condition with the positive feedback loop between continued immune cell activation and cytokine storm as the core mechanism to mediate multiple organ dysfunction. Inspired by macrophage membranes harbor the receptors with special high affinity for proinflammation cytokines, lipopolysaccharide (LPS)-stimulated macrophage membrane-coated nanoparticles (LMNP) were developed to show strong sponge ability to both IFN-γ and IL-6 and suppressed overactivation of macrophages by inhibiting JAK/STAT signaling pathway both *in vitro* and *in vivo*. Besides, LMNP also efficiently alleviated HLH-related symptoms including cytopenia, hepatosplenomegaly and hepatorenal dysfunction and save the life of mouse models. Furthermore, its sponge effect also worked well for five human HLH samples *in vitro*. Altogether, it's firstly demonstrated that biocompatible LMNP could dampen HLH with high potential for clinical transformation, which also provided alternative insights for the treatment of other cytokine storm-mediated pathologic conditions such as COVID-19 infection and cytokine releasing syndrome during CAR-T therapy.

1. Introduction

Hemophagocytic lymphohistiocytosis (HLH) is a rare, highly fatal condition with systematic inflammatory disorder and multiple organ dysfunction, which may arise from genetic defects (inherited form) and/or acquired risk factors (non-inherited form) such as infection (particular virus), autoimmune disease and malignancy (particular lymphoma) [1]. HLH is characterized by highly stimulated, but ineffective immune activation and subsequently cytokine storm. In all forms of HLH, T cells and macrophage/monocytes are continuously activated and accumulated in different organs such as the liver, spleen and bone marrow to release overwhelming cytokines, leading to various clinical symptoms including persistent fever, pancytopenia, hepatosplenomegaly and hepatorenal dysfunction [2,3].

The positive feedback loop between sustained, aberrant activation of inflammatory cells and cytokine storm is the core pathogenic mechanism underlying all forms of HLH. Indeed, hypercytokinemia is often associated with poor prognosis in HLH patients [4–6]. The treatments for HLH mainly include induction therapy and etiological therapy. The induction therapy alleviates cytokine storm-related symptoms, benefiting etiological therapy. The conventional induction therapies mainly involve chemotherapeutic agents (eg. etoposide) and immunosuppressive agents (eg. steroids and cyclosporine A), leading to inhibition of inflammatory cells and suppression of cytokine storm. However,

Peer review under responsibility of KeAi Communications Co., Ltd.
* Corresponding author.
** Corresponding author.
*** Corresponding author.
E-mail addresses: zqpang@fudan.edu.cn (Z. Pang), zhangbo19871987@126.com (B. Zhang), dr_huyu@126.com (Y. Hu).
[1] Equal contribution to the work.

https://doi.org/10.1016/j.bioactmat.2022.09.012
Received 5 January 2022; Received in revised form 12 August 2022; Accepted 9 September 2022

the efficacy of these treatments is low, as shown by 50% mortality in adults and children [7,8]. In addition, side effects associated with these treatments remain of great concern, as exemplified by increased risk of leukemia relapse caused by the treatment with topoisomerase inhibitors (eg. etoposide) [9].

Recently, targeted inflammation modulation, as a induction therapy for HLH, has attracted intensive attention [10]. Several cytokine antibodies against either IFN-γ, IL-6 or IL-1β [11] showed therapeutic

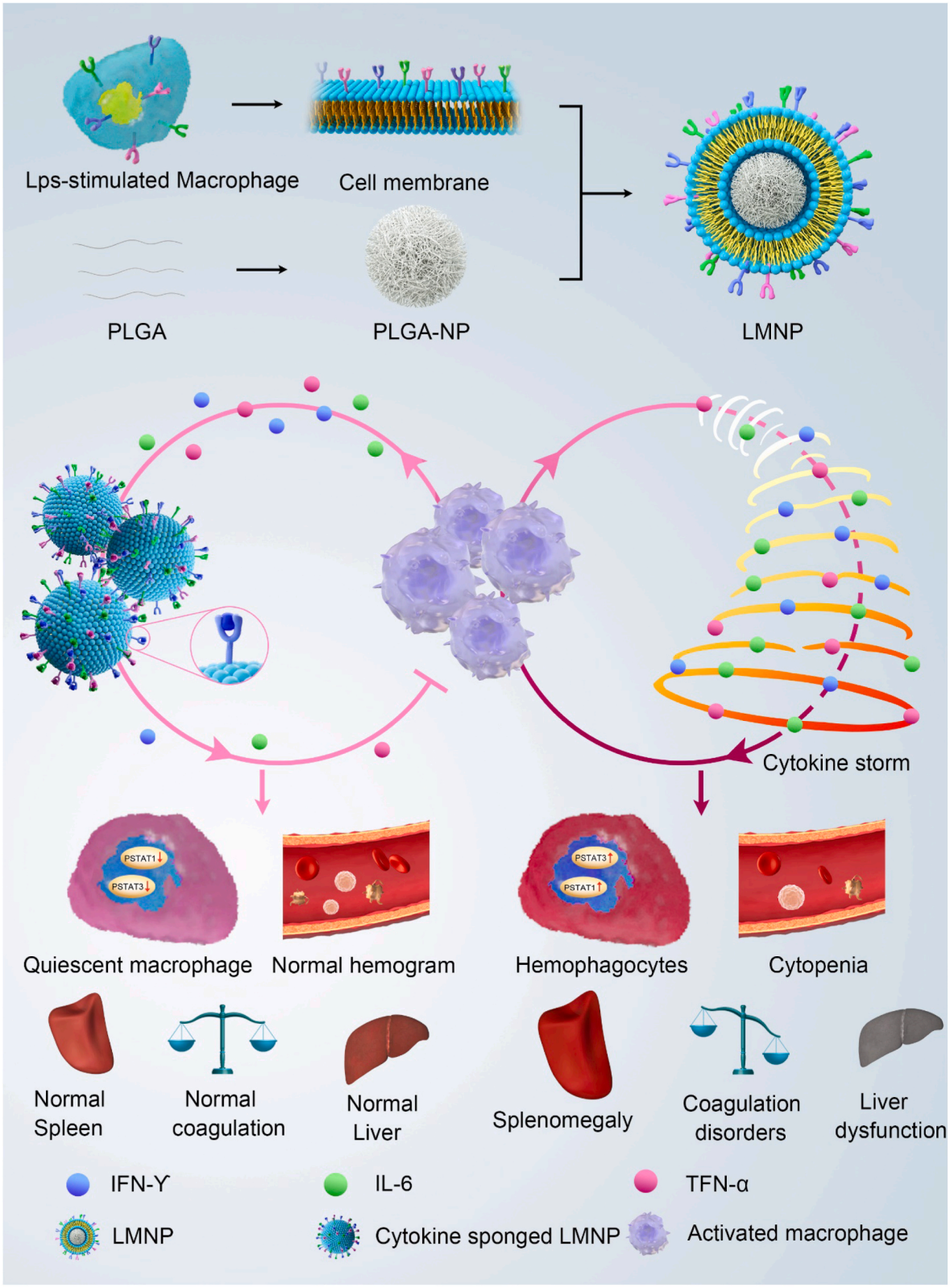

Scheme 1. Schematic illustration of the cytokine nanosponges (LMNP) suppressing overactive macrophages and dampening systematic cytokine storm for the treatment of hemophagocytic lymphohistiocytosis.

benefits in HLH patients to varying degrees. However, high cost of antibodies limits their wide use in clinics. Furthermore, one antibody can only target a specific cytokine, leading to less efficacy against cytokine storm involving multiple cytokines simultaneously [10]. In addition, some cytokine antibodies, such as IFN-γ antibody, may be associated with increased susceptibility to infections [12], which prevents their use from treating infection-induced HLH. Since activation of JAK/STAT pathway is responsible for excessive expression of multiple cytokines in HLH, ruxolitinib, a selective JAK1/2 inhibitor, was used to alleviate the symptoms of HLH in a murine HLH model [13] and in patients with refractory HLH [14]. Ruxolitinib shows better efficacy than the antibodies against cytokines, highlighting the benefit of immune-modulatory therapies that target multiple cytokines in the treatment of HLH. However, in clinics the remission depth of HLH by ruxolitinib is always not so sufficient [15–17]. Besides, the high cost of ruxolitinib and the likelihood to induce lymphoma and skin tumor might limit its wide use [18,19]. Together, alternative strategies with better cost-performance and the ability to target multiple cytokines with better safety are still urgently needed.

Cell membrane-coated nanoparticles that inherit the properties of source cells are recently emerging as a promising therapeutic platform [20–23]. For instance, red blood cell (RBC) membrane-coated nanoparticles showed favorable biocompatibility and prolonged circulation time compared with polyethylene glycol (PEG)-based nanoparticles [24]. RBC membrane-coated nanoparticles can also absorb different kinds of RBC-targeted agents such as pore-forming toxins [25], organophosphate poison [26] and pathological antibodies in autoimmune disease [27], leading to protection of healthy RBCs. In addition, neutrophil membrane-coated nanoparticles have been utilized to absorb cytokines and alleviate joint damage in inflammatory arthritis [28]. Macrophage membrane-coated nanoparticles displayed as a detoxification agent in a sepsis mouse model by binding and removing lipopolysaccharide (LPS) [29]. These reports suggest that inflammatory cell membranes with receptors for multiple cytokines maybe utilized to develop biomimetic nanoparticles and serve as a broad-spectrum anti--inflammatory agent to calm down the systematic cytokine storm in HLH.

With the advantage of easy preparation, high biocompatibility and excellent cost-performance, we developed, LPS-stimulated macrophage membrane-coated nanoparticles (LMNP) by coating cell membrane derived from LPS-stimulated macrophages onto a biodegradable polymeric nanoparticle core (Scheme 1). We further showed the affinity and clearance ability of LMNP to multiple types of inflammation cytokines and its subsequent efficacy on inhibiting overactive macrophages and the underlying mechanism both *in vitro* and *in vivo*. Besides, the effect of LMNP on the clinical manifestations caused by cytokine storm, such as cytopenia, hepatosplenomegaly and impairment of hepatorenal function, were also assessed in a CpG-induced HLH mouse model. Finally, the therapeutic benefit of LMNP on the polyinosinc-polycytidylic acid (Poly(I:C)) plus LPS-induced lethal HLH mouse model was further demonstrated by prolonged survival time. Our results show that LMNP can dampen HLH by suppressing the systematical cytokine storm and overactive macrophages, providing alternative strategy for the treatment of HLH.

2. Results and discussion

2.1. Characterization of LMNP

As LMNP is covered by macrophage membrane, the amount of cytokine receptors expressed on the macrophage membrane determine the cytokine-sponging capability of LMNP. In this study, murine RAW264.7 cells were used to generate cell membranes and the expression levels of cytokine receptors including IL-6R and IFN-γR on LPS-induced pro-inflammatory M1-type macrophages and IL-4-induced anti-inflammatory M2-type macrophages were investigated. It was found that LPS-induced M1-type macrophages expressed more IFN-γR and IL-6R than naïve macrophages and IL-4-induced M2-type macrophages by Western blot (Fig. 1A&B, Fig. S1) and flow cytometry (Fig. 1C–E). This might render M1-type macrophages stronger ability to release more cytokines than naïve macrophages and M2-type macrophages, which is consistent to the pro-inflammation nature of M1-type macrophages [30]. Thus, LPS-stimulated RAW264.7 cells with higher expression levels of cytokine receptors were used as cell membrane sources in subsequent experiments.

LMNP were synthesized by a two-step method described previously [29]. Firstly, the bare PLGA nanoparticle core (NP) was prepared by a precipitation method. Secondly, NP was coated with LPS-treated RAW264.7 cell membranes and naïve RAW264.7 cell membranes to form LMNP and MNP, respectively. LPS residues on LMNP were detected and the results demonstrated that LMNP was free of LPS (Fig. S2), which verified the high purity of LMNP. After synthesis, LMNP were uniformly dispersed and exhibited spherical shell-core structures under TEM and smooth round surfaces under Cryo-EM (Fig. 1F&G). Compared with NP, LMNP have a slightly increased diameter from 95.2 nm to 101.1 nm (Fig. 1H). LMNP performed −20.2 mV in surface zeta potential, which was equivalent to that of membrane vesicle derived from LPS-treated RAW264.7 cells (Vesicle) but slightly lower than that of NP (Fig. 1I). The average size of LMNP was consistent at around 100 nm over 7 days at 4 °C when suspended in 10% FBS (Fig. 1J). Both SDS-PAGE and Western blot demonstrated LMNP maintained the key membrane proteins of LPS-treated RAW 264.7 cells (Raw), including IFN-γR and IL-6R that were responsible for cytokine-sponging (Fig. 1K-N). We further confirmed that the cell membrane with the right-side-out protein orientation was coated onto the surface of NP through the identification of IFN-γR and IL-6R on the surface of NP by flow cytometry (Figure 1O, Fig. S3). Altogether, these results demonstrated that LMNP harbored an identical antigenic exterior as the source macrophages, and consequently inherited the ability of macrophages to bind with multiple types of cytokines, which would otherwise stimulate macrophages and other immune cells to produce more cytokines. The top-down fabrication of LMNP effectively replicates the key cytokine receptors and related moieties from the source macrophages and avoids the need for receptor identification, purification, and conjugation. To this end, LMNP may serve as a board-spectrum anti-inflammatory tool to alleviate the systematic cytokine storm in HLH.

2.2. Cytokine-sponging ability of LMNP in vitro

IFN-γ and IL-6 mediate the pathophysiological process of HLH [2,3]. Their expression levels were found to be increased in the circulation system of both primary and secondary HLH mouse models and clinical samples, and were correlated to the prognosis of HLH patients [13,31]. Indeed, antibodies against IFN-γ and IL-6 have already been approved for HLH treatment in clinics [3,10] and various success has been achieved in some case reports and clinical trial of HLH [32]. Therefore, IFN-γ and IL-6 were selected as the two representative markers for the evaluating the cytokine-sponging ability of LMNP. Due to the higher expression of IFN-γR and IL-6R on LPS-stimulated macrophage membranes, LMNP accordingly demonstrated a much stronger sponging ability to both IFN-γ and IL-6 compared with MNP (Fig. 2A&D). It's worth noting that the sponging capability of LMNP on IFN-γ was significantly reduced when IFN-γR antibody was used to block IFN-γR on the surface of LMNP while the reduction was not observed when nonspecific IgG was applied, indicating that the binding between LMNP and IFN-γ was IFN-γR-specific (Fig. S4). We then used LMNP in the following experiments. In addition, apart from the stimulation method used in this study, an alternative way to improve the cytokine-absorbing ability of the cell membranes might be the gene engineering technology which is capable of driving the expression of some particular receptors [33,34]. However, the gene engineering technology is more complex and of high price compared with the LPS stimulation method utilized in the present study.

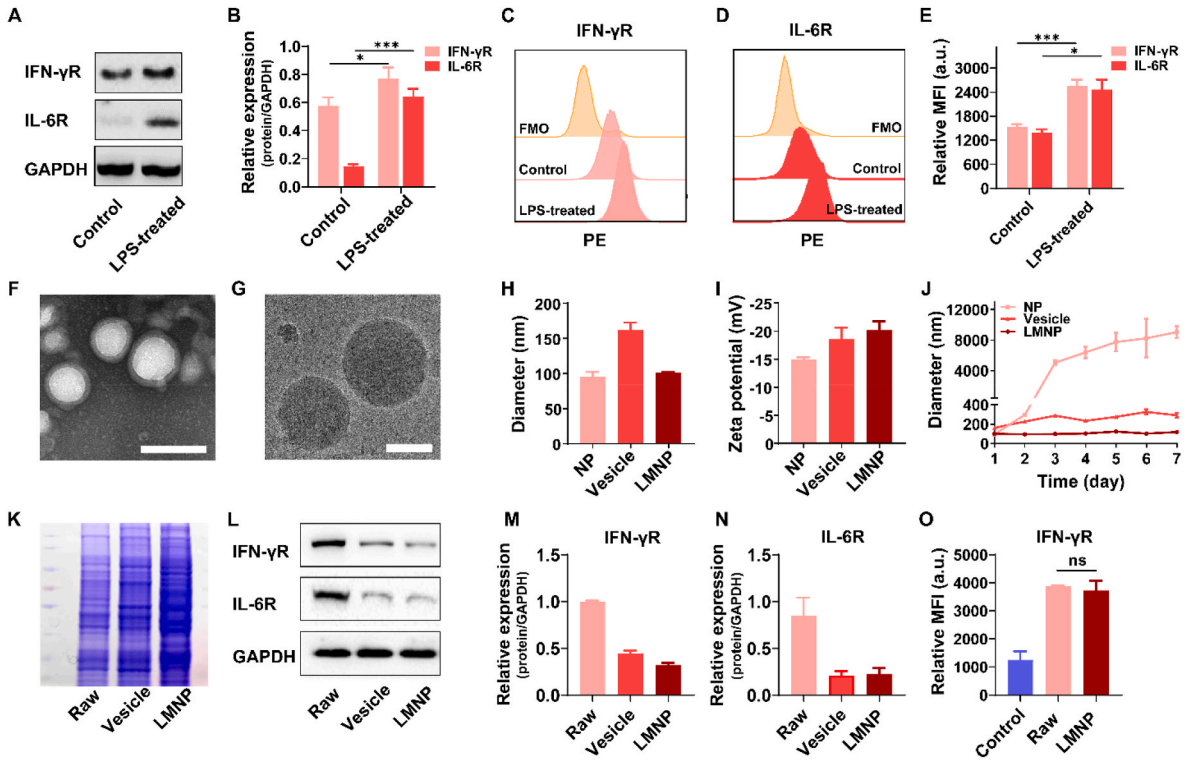

Fig. 1. Characterization of LMNP. (**A, B**) The expression of IFN-γR and IL-6R on macrophages treated with 10 ng/ml of LPS revealed by (**A**) Western blot and (**B**) the corresponding quantitative results analyzed by ImageJ (n = 3). (**C-E**) The representative flow histogram of (**C**) IFN-γR and (**D**) IL-6R expressions on macrophages treated with 10 ng/ml of LPS and (**E**) the corresponding quantitative results (n = 3). Macrophages without LPS treatment served as a control. FMO indicated LPS-treated macrophages without staining with PE-labeled antibody. IFN-γR and IL-6R was stained with PE-labeled anti-mouse IFN-γR antibody and PE-labeled anti-mouse IL-6R antibody, respectively. (**F, G**) The morphology of LMNP was observed under (**F**) transmission electron microscopy (TEM) and (**G**) cryo-electron microscopy (Cryo-EM). Scale bar = 100 nm. (**H**) The diameter and (**I**) the zeta potential of NP, LPS-treated RAW 264.7 cell membrane vesicles (Vesicle) and LMNP (n = 3). (**J**) The size stability of LMNP, NP and Vesicle over a span of 7 days in 10% FBS (n = 3). (**K**) Sodium dodecyl sulfate-polyacrylamide gel electrophoresis (SDS-PAGE) analysis of the proteins in the cell lysate of LPS-treated RAW264.7 cells (Raw), Vesicle and LMNP. (**L-N**) The expressions of IFN-γR and IL-6R in Raw, Vesicle and LMNP revealed by (**L**) Western blot and (**M, N**) the corresponding quantitative results analyzed by ImageJ (n = 3). (**O**) Comparison of mean fluorescence intensity from Raw and LMNP stained with PE-labeled anti-mouse IFN-γR antibody. LPS-treated RAW 264.7 cells without antibody staining served as a control (n = 3). MFI, mean fluorescence intensity. *$P < 0.05$, ***$P < 0.001$. The abbreviation "ns" indicated no significant difference.

We next investigated the sponging capability of LMNP to individual cytokines. The cytokines of known concentration were incubated with LMNP or its other counterparts, followed by ultracentrifugation to remove nanoparticles. The amounts of cytokines remaining in the supernatant were quantified by ELISA to calculate the sponging efficiency. When 500 pg of IFN-γ or IL-6 was incubated with different nanoparticles in 1 ml of deionized water, 0.5 mg of LMNP sponged 371 pg of IFN-γ and 347 pg of IL-6, respectively. The IFN-γ and IL-6 sponging efficiency of LMNP was 74.3% and 69.4%, respectively. They were significantly higher than those of its counterparts including NP, liposomes (Lip) and Vesicle (Fig. 2B&E). To investigate the effect of medium on the cytokine-sponging capability of LMNP, deionized water, mouse plasma, 10% FBS and PBS (0.01 M, pH = 7.4) (PBS) were tested. The results demonstrated LMNP had stronger cytokine-sponging ability of both IFN-γ and IL-6 in deionized water and mouse plasma compared with other mediums (Fig. 2C&F).

We next precisely quantify the capacity of LMNP to adsorb different types of cytokines. IFN-γ or IL- 6 at 500 pg/ml was incubated with LMNP of various concentrations ranging from 0 to 1000 μg/ml. LMNP sponged IFN-γ or IL-6 in a concentration-dependent manner in the tested dose range (Fig. 2 G&J). When LMNP solution at 500 μg/ml was incubated with IFN-γ or IL-6 of various concentrations from 0 to 1000 pg/ml, it was found that with the concentration of cytokines decreased, their amounts in the supernatant also declined but the removal efficiency of cytokines didn't change prominently, around 76.3% for IFN-γ and 63.1% for IL-6, respectively (Fig. 2H&K). The binding affinity (K_d) and the maximal binding (B_{max}) of LMNP to IFN-γ were 8346 pg and 14.17 pg/μg nanoparticles, respectively. The K_d and B_{max} of LMNP to IL-6 were 14044 pg and 18.54 pg/μg nanoparticles, respectively. Of note, there was no significant difference in the cytokine concentration in the supernatants when the incubation last for 0.5 h or 2 h (Fig. S5), indicating the fast sponging of IFN-γ or IL-6 by LMNP within 0.5 h and sponging effect was relatively stable within 2 h.

To further explore the translational potential of our LMNP, we evaluated the cytokine-sponging capability in the blood collected from HLH patients. LMNP could sponge around 40%–100% of IFN-γ in patients' serum. Strikingly, we observed 100% sponge of IFN-γ in 3 out of 5 patient samples (Fig. 2I). In comparison, we found about 20%–80% of IL-6 was sponged by LMNP in patient samples (Figure 2L). LMNP with murine IFN-γR and IL-6R on the surface worked well for both murine and human IFN-γ and IL-6, which could be partially explained by that murine IFN-γ, IL-6 and human IFN-γ, IL-6 were around 40% homology [35–37]. These results altogether indicated a potential clinical translation of our LMNP.

2.3. LMNP inhibits macrophage activation in vitro

Overactivation of inflammatory cells such as macrophages is a key characteristic of all types of HLH [2]. We next evaluated the effect of LMNP on cytokine-stimulated macrophages. IL-6 and IFN-γ were utilized to stimulate primary BMDMs, followed by isolation of $F4/80^+CD80^+$ population as the proinflammatory macrophages by flow

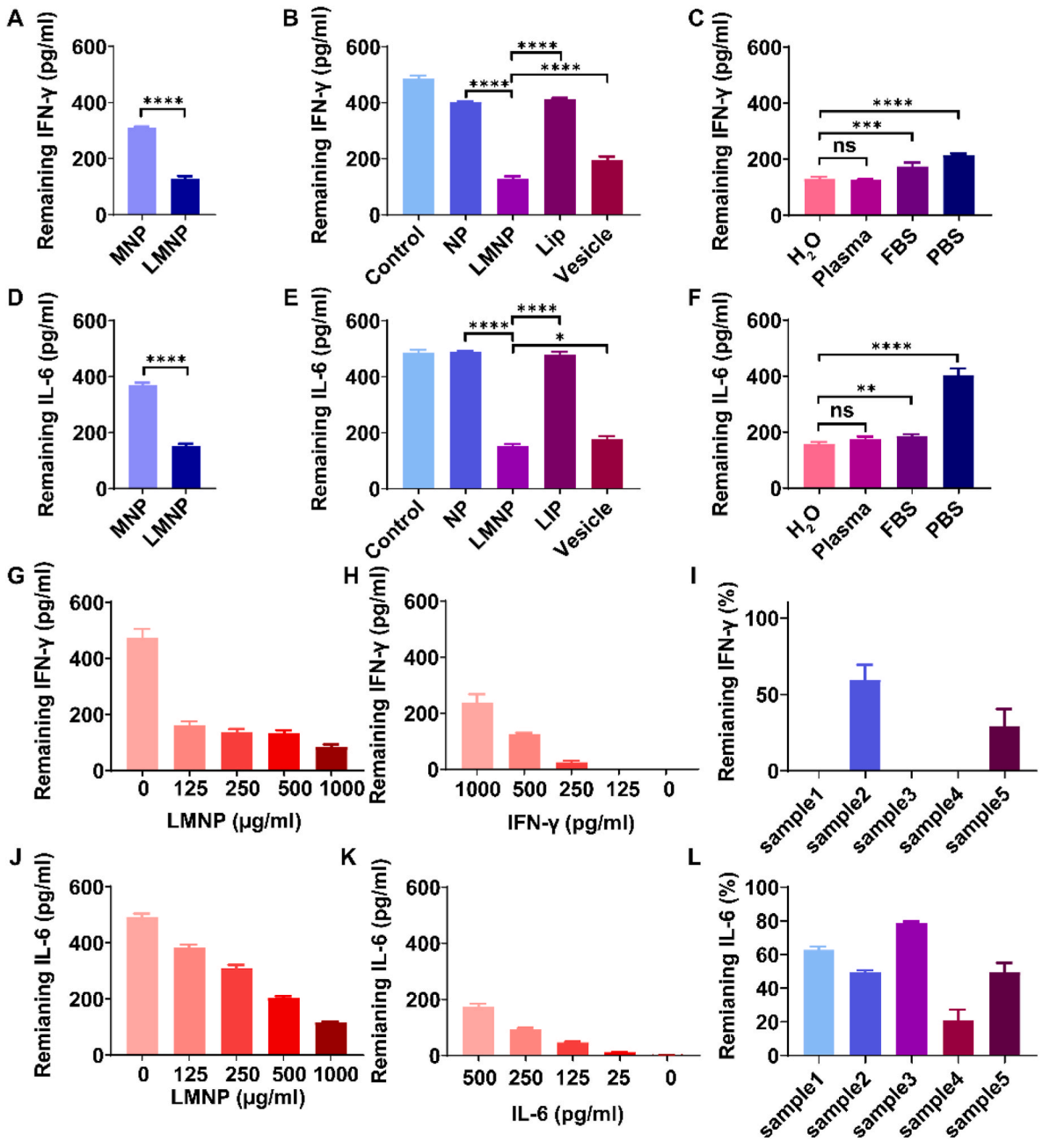

Fig. 2. Cytokine-sponging ability of LMNP *in vitro*. (**A**) IFN-γ removal with NP coated with LPS-stimulated macrophage membranes (LMNP) as compared with NP coated with non-LPS-stimulated macrophage membranes (MNP). (**B**) IFN-γ removal with LMNP, as compared with NP, Liposome (Lip), and the cell membrane vesicle derived from LPS-stimulated macrophages (Vesicle). (**C**) IFN-γ removal with LMNP in different mediums including denoised water, plasma, 10% FBS and PBS (0.01 M, pH = 7.4) (PBS). (**D**) IL-6 removal with LMNP as compared with MNP. (**E**) IL-6 removal with LMNP, as compared with NP, Lip and Vesicle. (**F**) IL-6 removal with LMNP in different mediums including denoised water, plasma, 10% FBS and PBS. (**G**) Quantification of IFN-γ removal in denoised water with IFN-γ (500 pg/ml) while varying amount of LMNP were added. (**H**) Quantification of IFN-γ removal with LMNP (500 μg/ml) while varying amounts of cytokines were added. (**I**) IFN-γ removal with LMNP in the serum of patient HLHs *in vitro*. (**J**) Quantification of IL-6 removal in denoised water with IL-6 (500 pg/ml) while varying amount of LMNP were added. (**K**) IL-6 removal with a fixed amount of LMNP (500 μg/ml) while varying amounts of cytokines were added. (**L**) IL-6 removal with LMNP in the serum of HLH patients *in vitro*. (n = 3), $^{*}P < 0.05$, $^{**}P < 0.01$, $^{***}P < 0.001$, and $^{****}P < 0.0001$. The abbreviation "ns" indicated no significant difference.

cytometry [38]. F4/80^{+}CD80^{+} population accounts for 17.6 ± 1.6% of cells in non-stimulated control group, whereas treatment with 10 and 100 pg/ml of IFN-γ elevated the percentages of proinflammatory macrophages to 29.5 ± 2.3% and 41.2 ± 0.5%, respectively. In contrast, LMNP treatment reversed the elevation of F4/80^{+}CD80^{+} population and decreased the percentage to 15.0 ± 0.2% and 20.7 ± 1.3%, respectively (Fig. 3A&B). Similarly, 10 and 200 pg/ml IL-6 treatment increased F4/80^{+}CD80^{+} population to 23.6 ± 1.3% and 27.4 ± 2.6%, respectively, compared with that for the control group (15.4 ± 0.7%), while further LMNP treatment completely reversed these effects (Fig. 3C&D).

We next explored the molecular mechanism underlying the effect of LMNP on suppressing overactivated macrophages. Transcriptome profiling of BMDMs treated with PBS, IFN-γ alone or IFN-γ plus LMNP were acquired by RNA-seq. Compared with the PBS group, we observed a significant upregulation of genes involved in macrophage activation, such as *Stat1, Stat2, Stat3, Irf1, Irf2, Irf8, Cd86, Cd40, Nos2, Nfkb1*, in the IFN-γ group [39–41]. In comparison, additional LMNP treatment (IFN-γ+LMNP group) abolished the upregulation of these genes

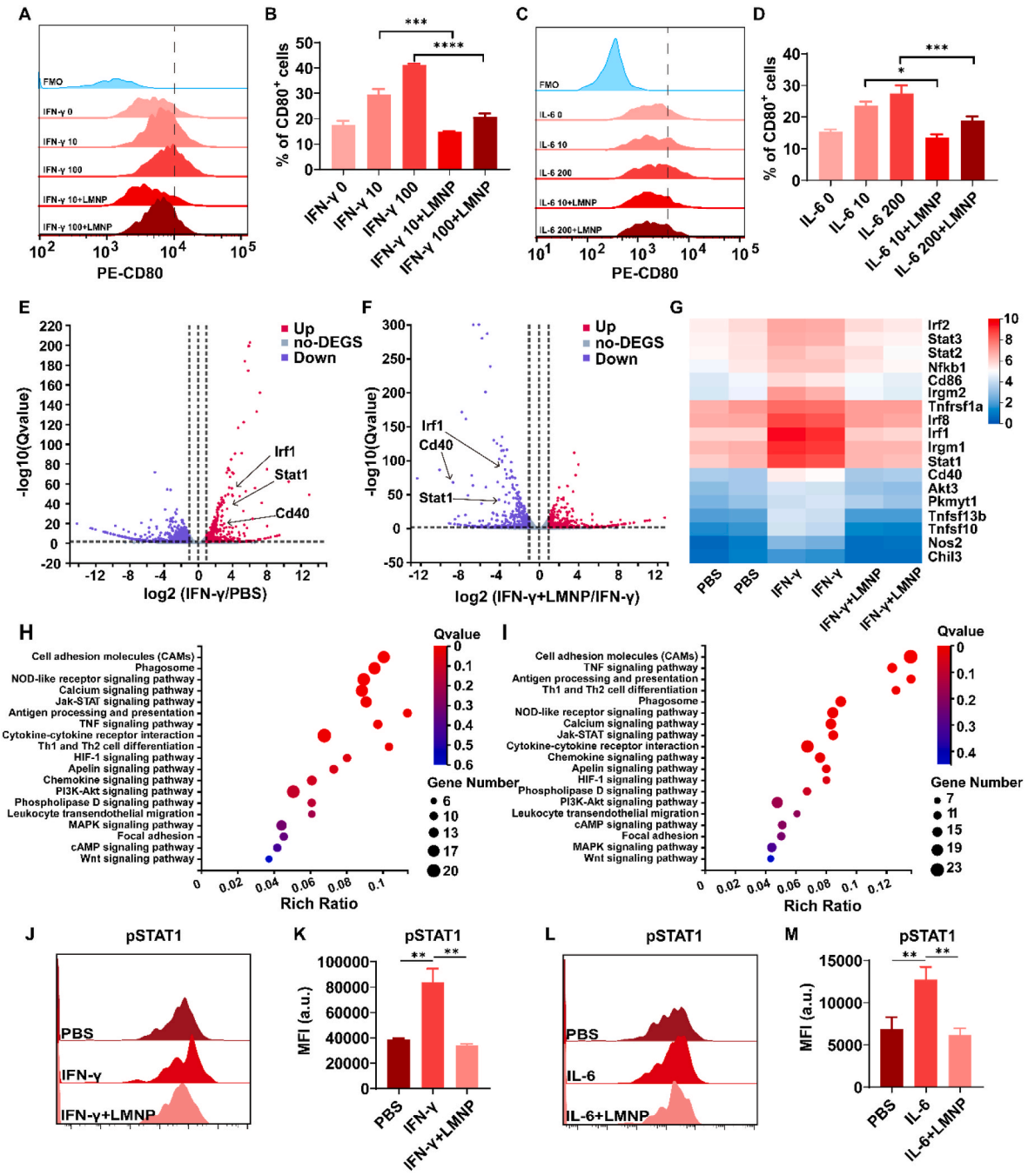

Fig. 3. LMNP inhibits macrophage activation *in vitro*. (**A-D**) Flow cytometry analysis of macrophage activation inhibited by LMNP. (**A&C**) Representative flow plots and (**B&D**) the corresponding quantification results of bone marrow-derived macrophages (BMDMs) treated with different concentrations of (**A&B**) IFN-γ pretreated with LMNP or (**C&D**) IL-6 pretreated with LMNP (n = 3). FMO indicated IFN-γ-stimulated macrophages without staining with PE-labeled CD80 antibody. IFN-γ 0, IFN-γ 10, and IFN-γ 100 indicated the IFN-γ concentration was 0, 10 ng/ml, and 100 ng/ml, respectively. IL-6 0, IL-6 10, and IL-6100 indicated the IL-6 concentration was 0, 10 ng/ml, and 100 ng/ml, respectively. (**E-I**) RNA sequencing analyses of macrophage activation inhibited by LMNP. (**E**) The differentially expressed genes (DEGS) between the IFN-γ group and the PBS group. (**F**) The DEGS between the IFN-γ pretreated with LMNP group (IFN-γ+LMNP) and the IFN-γ group. Log2FC ≥ 1 and $P < 0.001$. (**G**) Heatmaps illustrating the differentially expressed genes involved in macrophage activation among the PBS, IFN-γ and IFN-γ+LMNP groups based on RNA-seq analysis. (**H**) KEGG enrichment analyses identifying most significantly enriched pathways in the IFN-γ and PBS groups based on DEGS. (**I**) KEGG enrichment analyses identifying most significantly enriched pathways in the IFN-γ and IFN-γ+LMNP groups based on DEGS. (**J-M**) Flow cytometry analysis of pStat1 expression in macrophages after LMNP treatment. (**J&L**) The representative flow plot and (**K&M**) corresponding quantification results of pSTAT1 in $CD45^+F4/80^+CD80^+$ BMDMs treated with (**J&K**) IFN-γ+LMNP or (**L&M**) IL-6+LMNP (n = 3). *$P < 0.05$, **$P < 0.01$, ***$P < 0.001$, and ****$P < 0.0001$.

(Fig. 3E–G).

To further reveal the changes in signaling pathways, we performed KEGG analysis. Pathways linked to macrophage activation, including JAK/STAT, TNF, HIF-1, PI3K-Akt, MAPK and WNT signaling pathways, were significantly enriched in the IFN-γ group compared with the PBS group (Fig. 3H) [39–41]. Similar results were also observed in the IFN-γ group when compared with the IFN-γ+LMNP group (Fig. 3I). These results together indicated the state of BMDMs was similar between the PBS group and the IFN-γ+LMNP group.

JAK/STAT pathway is responsible for multiple cytokines production

and served as a therapeutic target for HLH in the clinic [14,42]. We then analyzed JAK/STAT pathway to validate the RNA-seq data. By flow cytometry, we observed an elevation in phosphorylated STAT1 (pSTAT1), a marker for JAK/STAT activation, in cells with IFN-γ or IL-6 stimulation. Additional LMNP significantly reduce the elevation (Fig. 3J-M). Multi-targets LMNP that target multiple macrophage activation-relevant pathways may exert a synergistic therapeutic effect and need further exploration in our future work.

2.4. LMNP benefit HLH treatment in the CpG-induced HLH mouse model

Several HLH mouse models has been previously reported, including the lymphocytic choriomeningitis virus (LCMV)-infected Prf1−/− mouse model [43], CpG-induced mouse model with or without α-IL-10 R treatment [44,45], LPS-induced mouse model based on senescence-accelerated mice [46] and poly (I:C) plus LPS-induced lethal mouse model [47]. All these mouse models had the main characterizations like clinical patients such as pancytopenia, hepatosplenomegaly, systematic cytokine storm with high levels of multiple types of inflammation cytokines in the circulation system and lymphoid tissues and the typical hematophagocytes. To investigate the therapeutic efficacy of LMNP in HLH, CpG-induced HLH mouse model was firstly used in our study due to its simplicity and low cost [45]. After five times of CpG treatment, pancytopenia, hepatosplenomegaly, increased level of inflammatory cytokine including IFN-γ, IL-6, IL-1β and TNF-α in the circulation system and local tissues and impairment of hepatorenal function were found in CpG treated mice compared with the control group, which were well consistent to previous studies [13,45]. In addition, hematophagocytes could also be found in the smear of spleen tissues in this HLH mouse model but not in the control group, which is a stronger indictor for HLH development. Altogether, all these evidences supported that the CpG-induced HLH mouse model has been successfully developed in the present study.

CpG-induced mouse models were treated with LMNP, MNP and NP at a dose of 2 mg/kg for ten days, and α–IFN–γ was used as a positive control as previously reported (Fig. 4A) [44,45]. We observed no

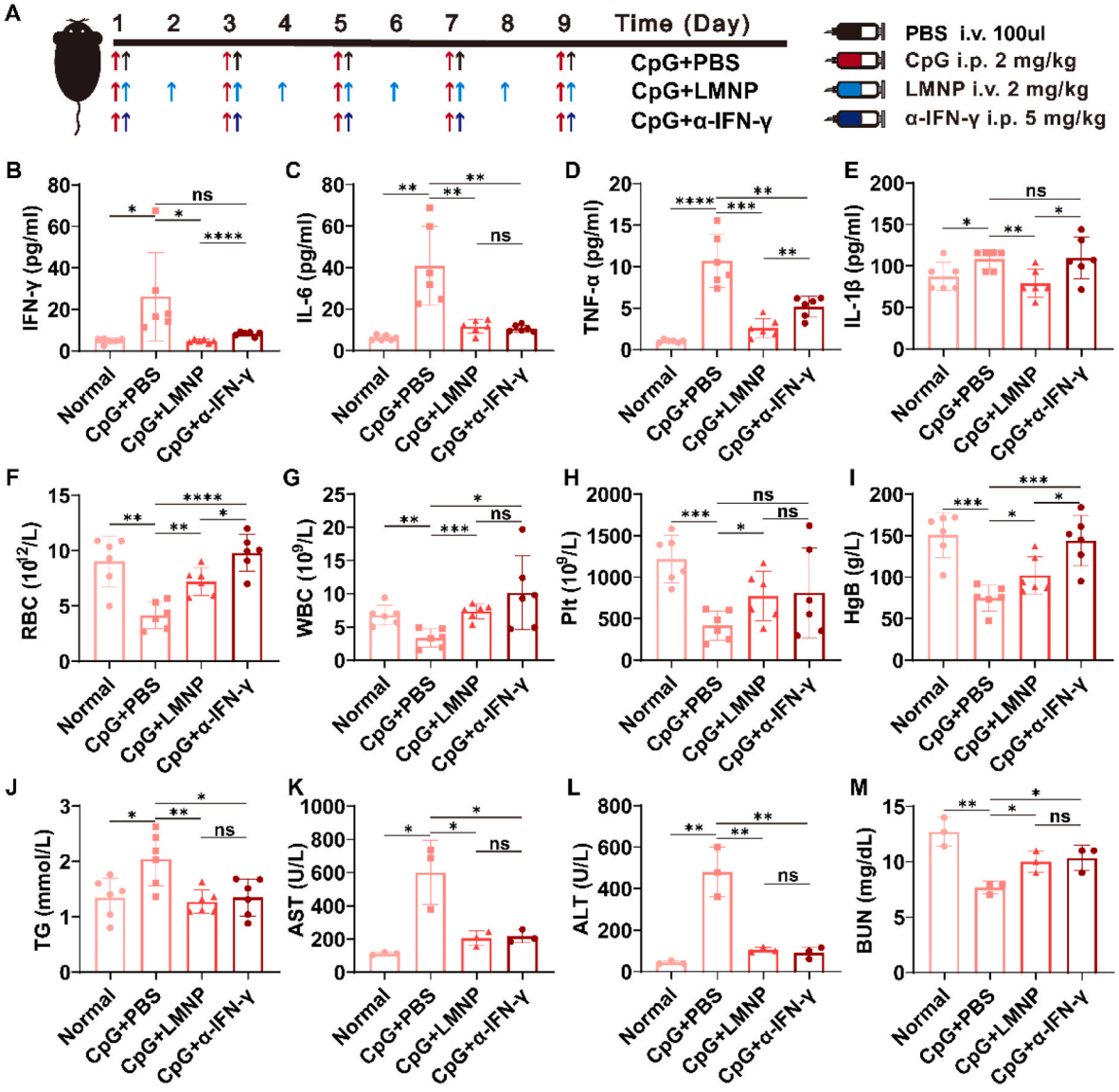

Fig. 4. LMNP treatment ameliorated hypercytokinemia and improved blood laboratory features of HLH. (**A**) Treatment schedules of different groups including PBS, LMNP, and IFN-γ antibody (α–IFN–γ) for CPG-induced HLH mouse models. (**B-E**) The effect of LMNP on cytokine storm were assessed by quantification of serum levels of multiple cytokines including IFN-γ (**B**), IL-6 (**C**), TNF-α (**D**) and IL-1β (**E**) (n = 6). (**F–I**) The effect of LMNP on cytopenia were investigated by blood routine test indicated by RBC (**F**), WBC (**G**), Plt (**H**), HgB (**I**) (n = 6). (**J-M**) The effect of LMNP on hepatorenal function indicated by TG (**J**), AST (**K**), ALT (**L**) and BUN (**M**) (n = 3). $^{*}P < 0.05$, $^{**}P < 0.01$, $^{***}P < 0.001$, and $^{****}P < 0.0001$. The abbreviation "ns" indicated no significant difference.

significant change in the body weight of mice during the timeframe of experiment (Fig. S6). Due to the critical role of cytokine storm in HLH development, we first evaluated the effect of LMNP on dampening cytokine storm, presented by overexpression of IFN-γ and its downstream, including IL-6, TNF-α and IL-1β [48]. The expression levels of these four cytokines in the serum samples, measured by ELISA, were significantly reduced by LMNP or α–IFN–γ treatment compared with PBS treated group (Fig. 4B–E). However, almost no significant reduction of cytokine concentrations in the serum was observed after MNP and NP treatment (Fig. S7I). Compared with α–IFN–γ treatment, LMNP treatment showed a significantly stronger effect in reducing the expression levels of IFN-γ, IL-1β, and TNF-α in the serum. However, there was no significant difference in the expression levels of the anti-inflammation cytokines such as IL-10 [48] between PBS treatment and LMNP treatment (Fig. S8).

Then the effect of LMNP treatment on systematic cytokine storm-related manifestations including pancytopenia, hepatosplenomegaly and impairment of hepatorenal function was assessed (Fig. 4F-M, Fig. 5). As compared with CpG-induced HLH mouse models treated with PBS, pancytopenia, in particular the counts of RBC, WBC, Plt and HgB were significantly increased after LMNP or α–IFN–γ treatment (Fig. 4F–I). In addition, the indicators of the hepatorenal function including TG, AST, ALT and BUN were significantly improved after LMNP or α–IFN–γ treatment (Fig. 4J-M). Besides, hepatosplenomegaly in the HLH mice was also significantly alleviated after LMNP or α–IFN–γ treatment. Compared with PBS treatment, the weight of spleen and liver after LMNP treatment was reduced by 48.8% and 20.9%, respectively (Fig. 5A&D, Fig. S9). The number of splenic cells as well as the proinflammatory macrophages were decreased by 28.7% and 56.5%, respectively, which were in line with the change of $F4/80^{+}$ positive inflammatory cells in the sections of spleen and liver tissues shown by IHC staining (Fig. 5C, E-G, Fig. S10). Intriguingly, we observed hemophagocytic cells in PBS treated HLH mice, but not in the normal mice and LMNP or α–IFN–γ treated HLH mice, suggesting LMNP or α–IFN–γ treatment could inhibit hemophagocytosis, which is consistent to the therapeutic benefits obtained by LMNP or α–IFN–γ treatment. As a comparison, HLH-related manifestations of CPG-induced HLH mouse models including pancytopenia, abnormal hepatorenal function, splenomegaly, proliferation and activation of macrophages, and hemophagocytosis were not found to be alleviated and improved after MNP and NP treatments (Fig. S7).

Besides, IHC staining also showed lower expression levels of IFN-γ and IL-6 in the liver and spleen tissues after LMNP or α–IFN–γ treatment compared with PBS treatment (Fig. 5H, Fig. S11&12). These results validated the capacity of LMNP to alleviate cytokine storm *in vivo*, which attributed to the capability of LMNP to bind IFN-γ and IL-6. Consequently, LMNP reduced the stimulatory effect of IFN-γ and IL-6 on macrophages, leading to less amounts of downstream cytokines. As JAK/STAT pathway was a main pathway responsible for multiple cytokine production and closely involved in the HLH development, the effect of LMNP treatment on JAK/STAT pathway was further investigated to understand the mechanism of cytokine storm alleviation by LMNP treatment. Flow cytometry analysis showed that LMNP treatment significantly reduced pSTAT1 and pSTAT3 in macrophages compared with PBS or α–IFN–γ treatment (Fig. 5I-L). Altogether, LMNP treatment could successfully inhibit macrophage activation and dampen cytokine storm by, at least partially, inhibiting JAK/STAT signaling pathway.

Overall, LMNP treatment presented an overall superior effect to inhibit cytokine storm, leading to alleviation in HLH-related manifestations including pancytopenia, hepatosplenomegaly, multi-organ dysfunction and the presence of typical hemophagocytic cells.

2.5. Anti-HLH efficacy in the lethal HLH model

To expand the application of LMNP in HLH, a lethal secondary HLH mouse model induced by Poly(I:C) plus LPS induction was tested (Fig. 6). The timeline of model establishment and drug administration in C57BL/6 J mice was illustrated in Fig. 6A. This model shows much more severe cytokine storm compared with the CpG-induced HLH mouse model (Fig. 6D–H) [47]. The expression levels of IFN-γ, IL-6 and TNF-α in the serum in this HLH mouse models were around 270–600 times fold higher than those in the CpG-induced HLH mouse models (Fig. 6D–G), which was well consistent to previous report [45,47] and might be the main reason for the short survival time of this HLH mouse models. All HLH mice died at around 12 h after induction of HLH. For LMNP treated mice, 33% of the HLH mice treated twice survived after 96 h. Amazingly, increasing the treatment to 4 times with a 2-h interval between each treatment, further boosted the survival rate to 100% (Fig. 6B). In contrast, α–IFN–γ treatment exerted no obvious improvement in survival rate of these mice. It did not prolong the survival time at a dose of 10 mg/kg once or just prolonged the survival time to around 17 h at a dose of 10 mg/kg for four times as compared with PBS treatment (Fig. 6B), which consisted well to previous studies [47,49].

In addition, hematophagocytes were observed in HLH mouse spleen after PBS treatment or α–IFN–γ treatment but not in those after LMNP treatment (Fig. 6C). And coagulation disorder indicated by PT, APTT and FIB was alleviated after LMNP treatment in contrast to PBS or α–IFN–γ treatment (Fig. 6I–K). To understand the mechanism of the therapeutic benefit obtained by LMNP treatment, the effect of LMNP on dampening cytokine storm was further explored. ELISA results demonstrated that the expression levels of IL-1β, TNF-α, IFN-γ and IL-6 in the serum of LMNP treated HLH mice were reduced by 44.3%, 78.9%, 82.4% and 64.0%, respectively, as compared with those of PBS treated HLH mice (Fig. 6D–G). As a protective cytokine, IL-10 concentration in the serum of LMNP treated HLH mice was increased by 84.1% when compared with that of PBS treated HLH mice (Fig. 6H). Consistent well to the survival curve, α–IFN–γ treatment almost exerted no inhibitive effect on cytokine storm (Fig. 6D–H). As a comparison, HLH-related manifestations of this lethal HLH mouse models including the powerful cytokine storm, the dysregulated coagulation parameter, hematophagoctosis, and the survival time were not significantly improved after MNP and NP treatments (Fig. S13).

In the present study, LMNP exerted a stronger inhibition than α–IFN–γ in the expression levels of multiple types of inflammation factors in both CpG-induced HLH mouse models (Fig. 4B–E) and Poly(I:C) plus LPS-induced HLH mouse models (secondary lethal secondary HLH mouse model) (Fig. 6D–G). Particularly, in the Poly(I:C) plus LPS-induced lethal HLH mouse model, LMNP could significantly extend the survival of mice, showing a better efficacy than α–IFN–γ (Fig. 6B).

These results again demonstrated the necessity of simultaneous modulation of multiple types of inflammation cytokines by using nanosponges. In addition, what needs to be noticed was that the therapeutic benefit of α–IFN–γ was mouse model type-dependent. It could only lesson cytokine storm and alleviate cytokine storm-related manifestation on CpG-induced HLH mouse models (Figs. 4 and 5), but almost exerted no therapeutic effect on Poly(I:C) plus LPS-induced lethal HLH mouse models (Fig. 6B). Besides, IFN-γ concentration in the serum of HLH patients was found to be varied greatly between patients (Fig. S14), ranging from extremely high to almost undetectable as previously reported [48], which further demonstrated that IFN-γ was not a universal target for all HLH patients and single drug treatment with α–IFN–γ might not effectively manage HLH and save patients' life. Thus, the reasons for the superior therapeutic benefit of LMNP on HLH could be summarized as following. As a board-spectrum anti-inflammation agent, LMNP could remove IFN-γ and IL-6 or other cytokines in the circulation system and HLH-related organs, especially the liver and the spleen, which can then reduce the stimulation of IFN-γ and (or) IL-6 to macrophages and therefore less cytokines were produced by macrophages. And inhibition of macrophages activation in the liver could help restore normal liver function (Fig. 4J-M) [50]. As a comparison, antibody targeting only one single type of cytokines was not sufficient for dampening HLH [49] in which multiple different types of cytokines were involved. LMNP could

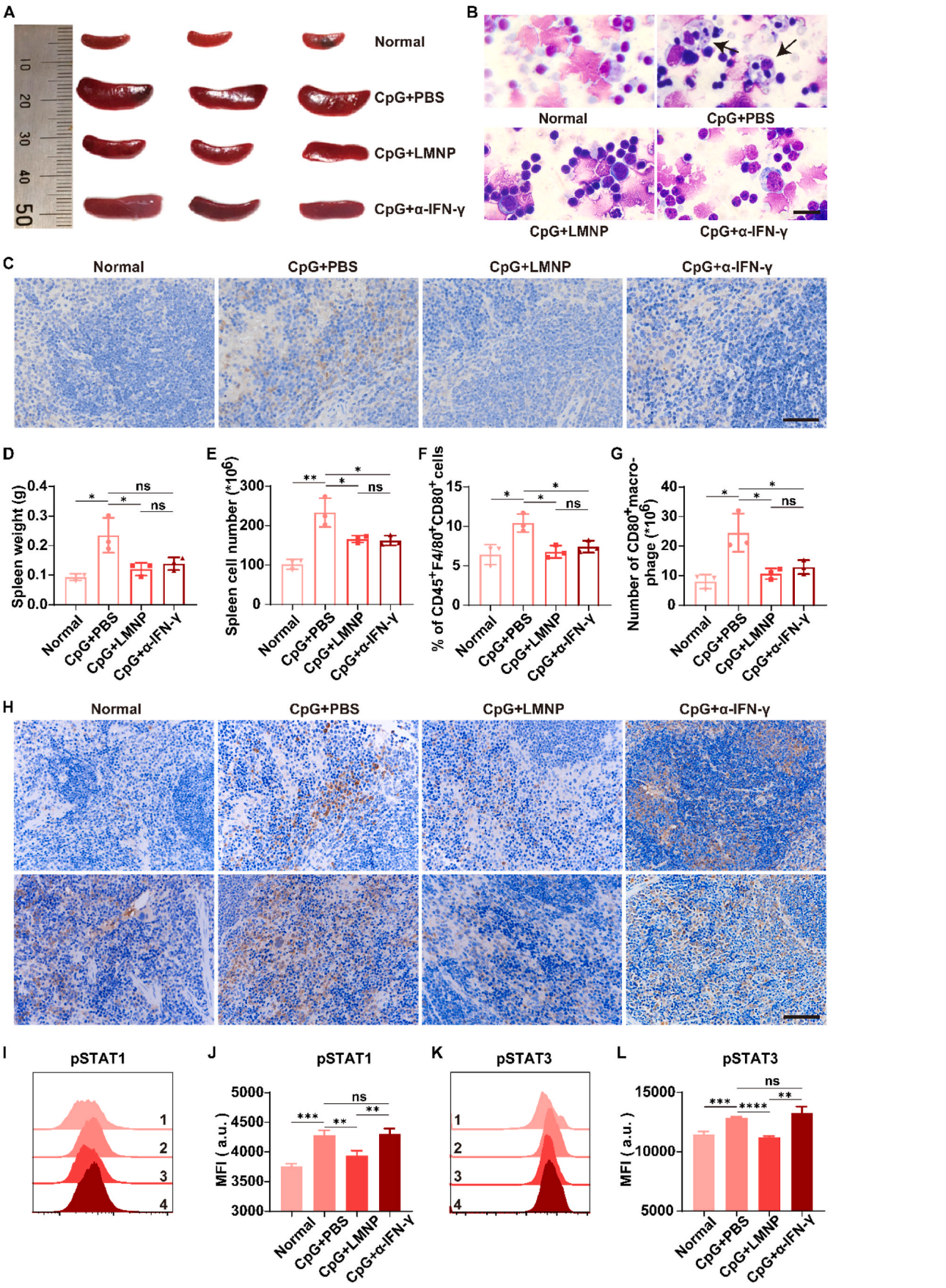

(caption on next page)

Fig. 5. Reduced macrophage activation *in vivo* through LMNP treatment. (**A**) Image of spleen from normal mouse group and different treatment groups for CPG-induced HLH mouse models including PBS, LMNP and α–IFN–γ groups. (**B**) The representative images of Liu's staining of smear of splenocytes. The arrow indicated the hemophagocytes. Bar = 20 μm. (**C**) The representative image of $F4/80^+$ cells in spleen sections by IHC staining. Bar = 50 μm. (**D-G**) The wet weight of spleen (**D**), the total splenic cell numbers (**E**), the percentage (**F**) and absolute number (**G**) of splenic $CD45^+F4/80^+CD80^+$ macrophages from different treatment groups (n = 3). (**H**) The representative images of IFN-γ (the upper panel) and IL-6 (the lower panel) expression in spleen tissues by IHC staining of spleen sections. (**I-L**) The representative flow plot (**I&K**) and corresponding quantification results (**J&L**) of pSTAT1 and pSTAT3 in macrophages (n = 3). $^*P < 0.05$, $^{**}P < 0.01$, $^{***}P < 0.001$, and $^{****}P < 0.0001$. The abbreviation "ns" indicated no significant difference.

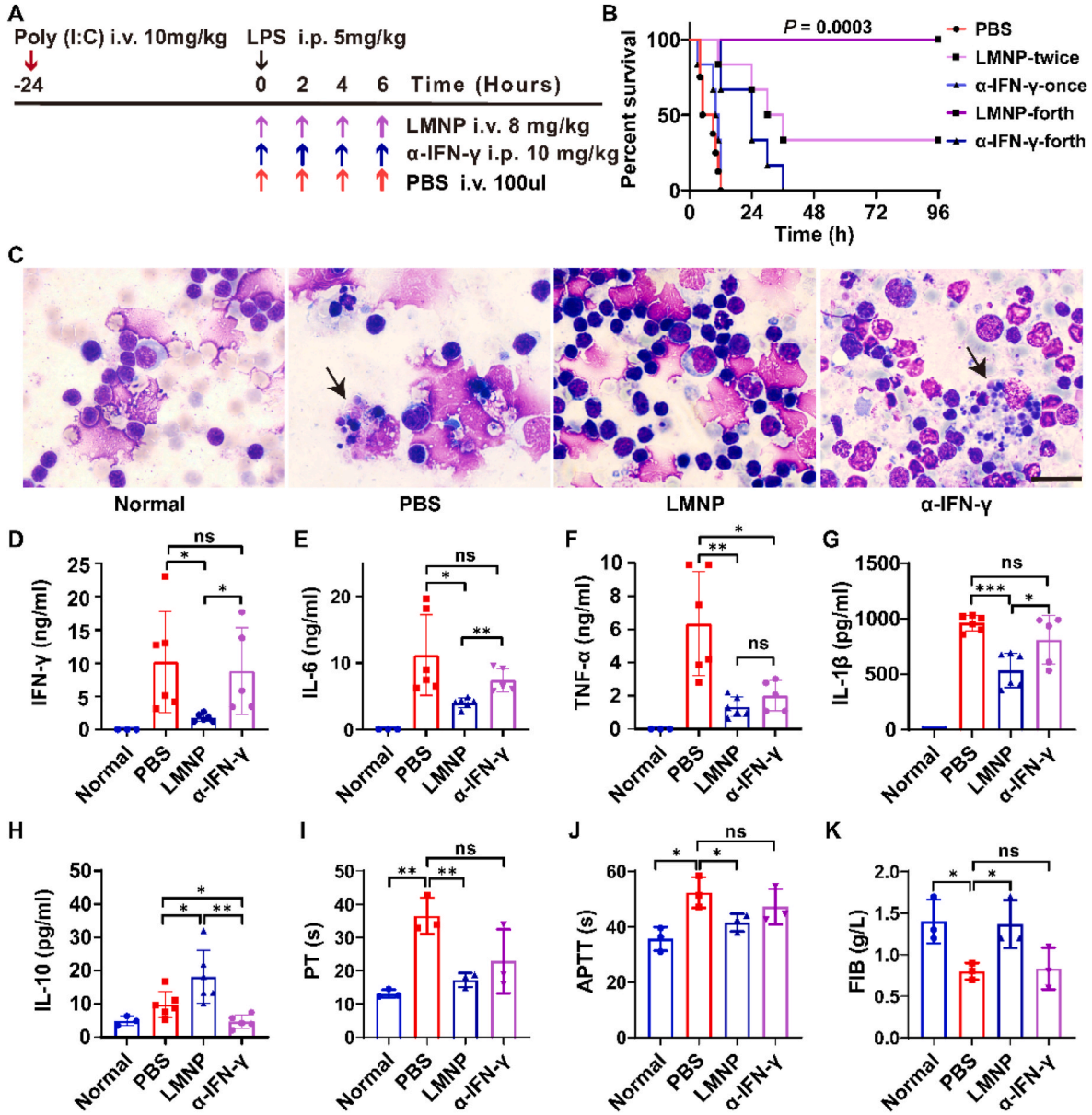

Fig. 6. Anti-HLH efficacy in the lethal HLH model. (**A**) Treatment schedules of different groups including PBS, LMNP, and α–IFN–γ for poly (I:C) and LPS-induced HLH mouse model. (**B**) Survival curves of HLH mouse model treated with LMNP, α–IFN–γ or PBS (n = 5). (**C**) The representative images of Liu's staining of smear of splenocytes. The arrow indicated the hemophagocytes. Bar = 50 μm. (**D-H**) The effect of LMNP on cytokine storm were assessed by quantification of serum levels of multiple cytokines including IFN-γ (**D**), IL-6 (**E**), TNF-α (**F**), IL-1β (**G**) and IL-10 (**H**) (n = 6). (**I–K**) The effect of LMNP on coagulation function including PT (I), ATPP (J), FIB (K) (n = 3). $^*P < 0.05$, $^{**}P < 0.01$ and $^{***}P < 0.001$. The abbreviation "ns" indicated no significant difference.

successfully interrupt the positive feedback loop between systematic cytokine storm and overactive macrophages, which was the core mechanism underlying HLH development. Therefore, the positive feedback loop interruption and cytokine storm alleviation by LMNP treatment (Figs. 4 and 6) was accompanied with improved parameters of blood routine test, reduction of the size of liver and spleen, less impairment of hepatorenal function, disappearance of hemophagocytic cells (Figs. 4 and 5) and prolonged survival time of mouse models (Fig. 6). Almost no therapeutic benefits were obtained in the MNP and NP groups in both CPG-induced HLH mouse models and the lethal HLH mouse models, which further demonstrated the specificity of LMNP in the present study (Figs. S7 and 13).

2.6. Biocompatibility and pharmacokinetics of LMNP

Finally, we investigated the biocompatibility and pharmacokinetics of LMNP. Normal mice were employed for this study. We observed no obvious difference in the expression of inflammation cytokines including TNF-α, IL-1β, IFN-γ and IL-6 between PBS and LMNP treated group (Fig. 7A–D). In addition, we observed no abnormality in the blood of LMNP mice, as shown by RBC, WBC, Plt and HgB counts, and biochemistry test such as TG, AST, ALT and BUN (Fig. 7E-L). Furthermore, no obvious damage was observed in the major organs including the heart, liver, spleen, lung and kidney by H&E staining (Figure 7M). Altogether, these results indicated a favorable biocompatibility of LMNP treatment in mice. According to the pharmacokinetic results (Fig. S15), LMNP and NP showed 16.8% and 6.4% retention in the blood at 24 h after injection, respectively. The clearance of LMNP was much slower than NP in the blood, consistent with the fact that the macrophage membrane coating could prolong the circulation time of nanoparticles [21]. LMNP was distributed mainly in the liver and the spleen (Fig. S15), suggesting that it is mainly cleared through the mononuclear phagocyte system, which consisted well to previous reports [51,52].

It was previously reported that biomimetic nanoparticles, taking advantage of the inflammation targeting ability of platelet membranes or macrophage membranes, could deliver anti-inflammation agents [5-(*p*-fluorophenyl)-2-ureido] thiophene-3-carboxamide (TPCA-1) or tacrolimus to the inflammation sites in mouse lung caused by acute injury or rheumatoid arthritis [20,21,38]. Besides, nanoparticles coated by cell membranes derived from macrophages or neutrophils could also bind and remove inflammation factors in sepsis and arthritis mouse models [28,29]. Previous studies mainly focus on inhibiting inflammation response in local sites such as tumors, acute lung injury, arthritis, heart injury and inflammatory bowel diseases [28,38,53–55], while the effect on controlling systematic cytokine storm using biomimetic nanoparticles were largely unknown. To the best of our knowledge, this study, showed that LMNP, which are nanoparticles coated with cell membrane derived from activated macrophages, could calm down systematic cytokine storm in HLH. LMNP thus represents a promising strategy to improve the treatment of HLH by potentially shifting the current cytotoxic chemotherapy and immunosuppression paradigm towards the multiple-target immune modulation therapy. Apart from macrophages, T lymphocytes, dendritic cells and neutrophils are also involved in the cytokine storm loop in HLH [3,13]. It will be interesting to explore whether biomimetic nanoparticles based on these cell membranes show similar effect in the treatment of HLH.

Studies about the inflammatory factor profile in HLH are attracting extensive attention nowadays, which not only helps distinguish HLH and other severe pathologic conditions like sepsis, but also contributes to seeking alternative therapeutic targets or disease monitoring markers for HLH. Many inflammatory factors including IFN-γ, IL-6, TNF-α, IL-1β, and IL-10 were reported to be elevated in HLH to various degrees. Some success has already been achieved by using antibodies for IFN-γ or IL-6 in HLH case reports and clinical trials [12,32]. Therefore, IFN-γ and IL-6 were selected as the main subjects in the present study. In addition, other inflammation factors such as C-X-C motif chemokine ligand 9 (CXCL9), CXCL10, G-CSF, and MIP-α were also reported to be increased in both primary and secondary HLH animal models [44]. CXCL9, an IFN-γ-induced chemokine, the serum level of which has also been showed to associate with the severity of HLH patients [56] and has been used as a marker to evaluate the efficacy of IFN-γ antibody in HLH clinical trials [12]. The two HLH mouse models presented in this study had significantly elevated IFN-γ, so we did not detect the level of CXCL-9. To facilitate clinical transformation of our study, it is desirable to detect serum CXCL-9 levels as well. Besides, inflammation factor pattern analysis of HLH by integrating different types of inflammation factors might provide a more elaborate tool for disease severity and therapeutic efficacy evaluation.

As recently reported, IL-6 binding to membrane-bound IL-6R could activate classical signaling mainly on immune cells, and it could also initiate trans signaling when binding to soluble IL-6R (sIL-6R) in other organs including the lung and the nervous system [57,58], which could also be attacked by the systematic cytokine storm in HLH patients [59]. Based on this important finding, it is believed that LMNP in the present study could block the membrane-bound IL-6R-associated classical signaling and also the sIL-6R-mediated trans signaling, which work together to relieve HLH-related manifestations.

Cytokine storm can arise from different pathologic conditions like HLH [11], SARS [49], coronavirus disease 2019 (COVID-19) [60], Castleman disease [61] and some intragenic situations such as the cytokine releasing syndrome during CAR-T therapy [11,62], radio therapy [63] and monoclonal antibody [64] treatments. As cytokine storm is a core pathogenic mechanism leading to multi-organ damage, accelerated calming down the cytokine storm is expected to improve the prognosis. Our LMNP not only provides an alternative strategy for HLH treatment, but also may benefit the treatment of a range of systematic cytokine storm-related diseases as mentioned above, providing different insights for the treatment of these diseases.

3. Conclusions

HLH represented a highly fatal disease characterized by aberrant activation of inflammation cells and resultant cytokine storm with a dismal prognosis. A biomimetic activated macrophage membrane-coated LMNP was successfully developed to serve as alternative treatment for the management of HLH. LMNP could sponge multiple types of inflammation cytokines, leading to superior therapeutic effect for HLH treatment in both mild and lethal HLH mouse models. In addition, its sponge effect also worked well for human HLH samples, and the biocompatible nature of LMNP further support its potential for clinical translation. The strategy proposed by this study also provides insights for the management of other systematic cytokine storm-based pathologic conditions such as COVID-19 and cytokine releasing syndrome during CAR-T therapy.

4. Materials and methods

4.1. Materials and animals

CpG 1826 oligonucleotide was synthesized by Sangon Biotech (Shanghai, China), TNF-α, IL-1β, IL-10, IL-6 and IFN-γ ELISA kits were obtained from MultiSciences Biotechnology Co., Ltd. (Hangzhou, China). The mouse LPS ELISA kit was acquired from Jianglai Biotechnology (Shanghai, China). Egg yolk lecithin (EPC, PL-100 M) and 1,2-distearoyl-sn-glycero-3-phosphoethanolamine-N-[methoxy(polyethylene glycol)-2000] (DSPE-PEG2000) were purchased from AVT Pharmaceutical Tech Co., Ltd. (Shanghai, China). Ultra-LEAF™ Purified anti-mouse IFN-γ antibody (α–IFN–γ), mouse IFN-γR antibody, Cytofix/Cytoperm Kit and fluorochrome-conjugated anti-mouse antibody (Pacific Blue™-CD45, PE-CD80, APC-F4/80, PerCP/Cyanine5.5-pSTAT1, FITC-pSTAT3, PE–IFN–γR and PE-IL-6R) were purchased from Biolegend (San Diego, CA, USA). Fetal bovine serum (FBS), dulbecco's modified eagle medium (DMEM) and penicillin–streptomycin were from Gibco (Carlsbad, CA, USA). Carboxyl group-terminated poly(lactide-co-glycolide acid) (PLGA) (lactide: glycolide monomer ratio of 50:50) was from Corbion Purac (Netherlands). Plastic cell culture dishes and plates were supplied by Corning Incorporation (Corning, NY, USA). Deionized water was acquired from the Millipore Simplicity System (Millipore, Bedford, MA, USA). Laser confocal Petri dish was ordered from Absin Biological Technology Co., Ltd. (Shanghai, China). Liu's stain was purchased from BaSO Biological Technology Co., Ltd. (Zhuhai, China). Recombinant murine macrophage colony stimulating factor (M-CSF), IL-6, IL-4 and IFN-γ were from PeproTech (Cranbury, NJ, USA). High molecular weight Poly (I:C) was purchased from InvivoGen (USA). LPS and cholesterol was obtained from Sigma (USA). BCA protein assay kit

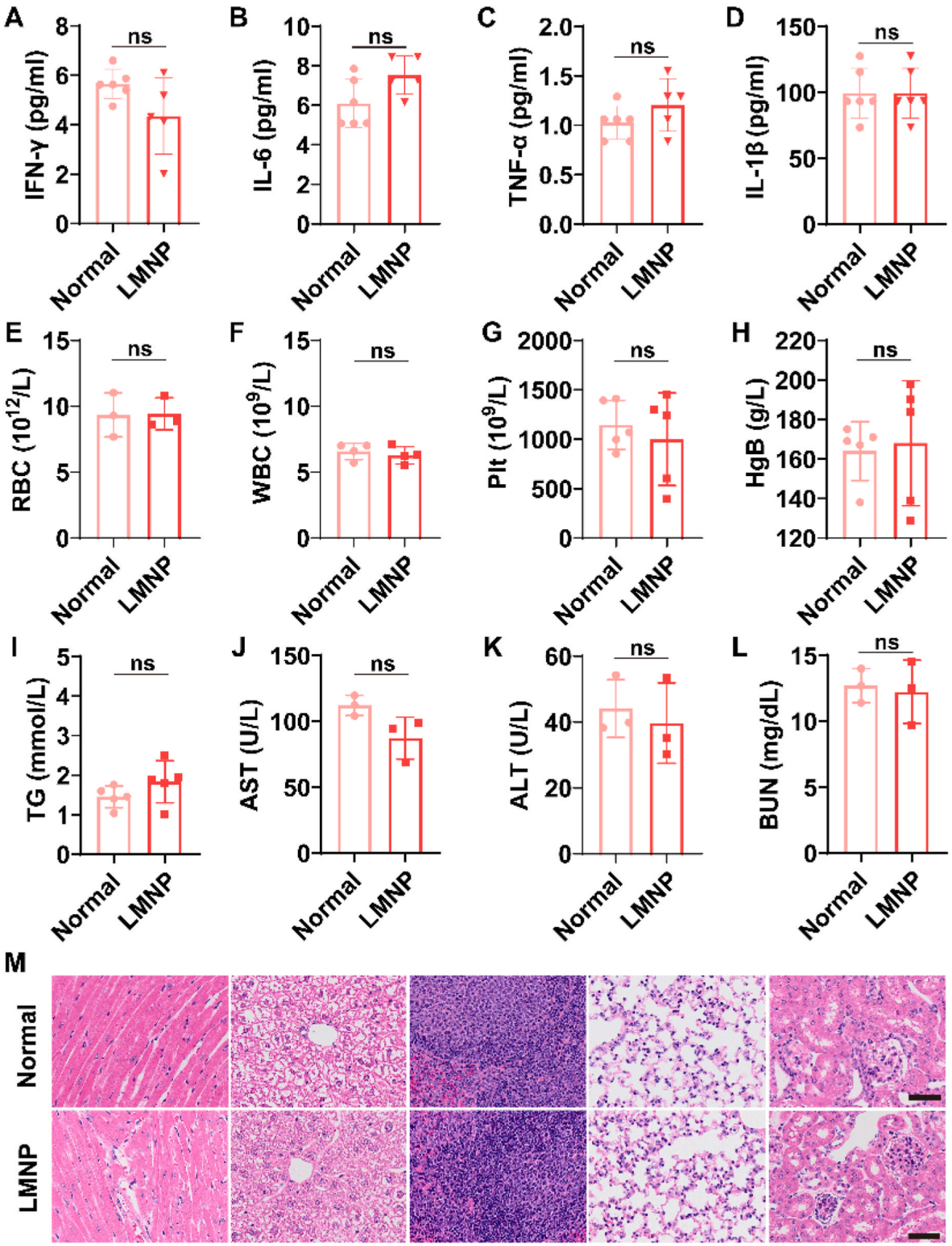

Fig. 7. The safety and biocompatibility of LMNP. (**A-D**) The cytokines level in mouse serum from Normal and LMNP treated groups including IFN-γ (**A**), IL-6 (**B**), TNF-α (**C**) and IL-1β (**D**) (n = 5). (**E-L**) Blood routine test (**E-H**) and hepatorenal function (**I-L**) of mice from LMNP and control groups. Blood routine test was indicated by RBC (**E**), WBC (**F**), Plt (**G**) and HgB (**H**). The hepatorenal function was indicated by TG (**I**), AST (**J**), ALT (**K**) and BUN (**L**) (n = 3). (**P**) The representative H&E images of major organs (from left to right: heart, liver, spleen, lung, kidney) at the endpoint of treatment (Bar = 50 μm). The abbreviation "ns" indicated no significant difference.

and 1,1′-Dioctadecyl-3,3,3′,3′-Tetramethylindodicarbocyanine,4-Chlorobenzenesulfonate Salt (DiD) were purchased from Beyotime Biotechnology Co. Ltd. (Nantong, China). Protease inhibitor cocktail (PierceTM Protease Inhibitor Mini Tablet) was obtained from Thermo (Rockford, USA). The other chemicals and reagents of analytical reagent grade were purchased from Sinopharm Chemical Reagent (Shanghai, China).

Murine RAW264.7 cell line was obtained from the Chinese Academy of Sciences Cell Bank (Shanghai, China), and was cultured in DMEM containing 10% FBS at 37 °C and 5% CO2. Male C57BL/6 J mice aged six weeks were obtained from Lingchang Biotech (Shanghai, China), and all mice were raised in the Center for Experimental Animals at School of Pharmacy, Fudan University. The animal experimental protocol was approved by the Animal Ethics Committee of Fudan University in compliance with national and institutional guidelines.

4.2. Macrophage membrane derivation and characterization

To determine whether cytokine receptor expression enriched in RAW264.7 after LPS treatment, IFN-γR and IL-6R expressions of whole cell lysate were assessed by Western blot as previously described [29]. In brief, RAW264.7 cells were stimulated with LPS at a dose of 10 ng/ml for 24 h, besides cells without LPS treatment served as a control. Then cells were lysed using RIPA buffer. After protein quantification by BCA kit, the cell samples with equal amount of proteins were separated using sodium dodecyl sulfate-polyacrylamide gel electrophoresis (SDS-PAGE), underwent electrophoresis and blocking, incubated with primary antibodies for IFN-γR or IL-6R overnight at 4 °C, followed by washing 3 times with TBST (10 mM Tris, pH 7.5, 0.2% Triton X-100 and 150 mM NaCl), exposed to corresponding secondary antibodies, and detected by using Immobilon™ Western Chemiluminescent HRP Substrate (Millipore). The band density of the scanned blots was analyzed by using Image J and the expression of IFN-γR or IL-6R relative to the internal parameter (GAPDH) was calculated. The cells were also stained with PE-labeled primary antibodies for IFN-γR or IL-6R and subjected to flow cytometry according to the standard protocol to evaluate the expression level of IFN-γR or IL-6R on the cell membranes.

For macrophage membrane deviation, RAW264.7 cells treated with LPS or not were collected and washed in PBS (0.01 M, pH 7.4) (PBS) for 3 times, and grinded in 10 ml of hypotonic fluid (75 mM sucrose, 20 mM Tris·HCl, pH 7.5; 2 mM $MgCl_2$; 10 mM KCl) supplemented with one table of protease inhibitor cocktail, and then centrifuged at 3200×*g* for 5 min. The collected supernatant was centrifuged at 20,000×*g* for 20 min, after which the collected supernatant was further ultracentrifuged at 100,000×*g* for 35 min in a centrifuge (CP100NX, Hitachi, Japan). After centrifugation, the supernatant was discarded and off-white precipitation was collected as macrophage membranes which was quantified with BCA assay reagents to identify the protein concentration. The macrophage membrane was finally suspended in the hypotonic fluid and stored in −80 °C for further use.

4.3. Preparation and characterization of LMNP

LMNP was prepared as previously described [21]. Firstly, PLGA polymer was dissolved in acetone at a concentration of 10 mg/ml. Then 500 μl of the solution was rapidly injected into 1 ml of water followed by vacuum evaporation to remove acetone and form the bare PLGA nanoparticle core (NP). Secondly, LPS-treated macrophage membranes containing 2.5 mg of membrane proteins were added to NP and sonicated in an ice bath for 5 min to synthesis LPS-treated macrophage membrane-coated NP (LMNP). LPS-treated macrophage membrane vesicles (Vesicle) were prepared with the same procedures as LMNP in the absence of NP. Naïve macrophage membranes without LPS stimulation were used to develop naïve macrophage membrane-coated NP (MNP) as a counterpart control.

The morphology of LMNP was observed under the transmission electron microscopy (TEM) (JEOL JEM-2010, Tokyo, Japan) after staining with uranyl acetate (1%) and cryo-electron microscopy (Cryo-EM) (Tecnai G2 F20; FEI, Eindhoven, The Netherlands) under liquid nitrogen. Size distribution and zeta potential of NP, Vesicle and LMNP were measured by using dynamic light scattering (ZEN3600 Zetasizer, Malvern, UK). The change of the size of LMNP, NP and Vesicle in 10% FBS was measured during one week as an indicator of stability.

4.4. Analysis of protein composition and orientation

The SDS-PAGE was utilized to confirm the proteins in the cell lysate of LPS-treated RAW264.7 cells (Raw), Vesicle and LMNP. The expressions of IFN-γR and IL-6R on Raw, Vesicle and LMNP were also identified by Western blot. The protocol was described in detail as aforementioned.

The orientations of IFN-γR and IL-6R on LMNP were identified by flow cytometry. In brief, LMNP were incubated with PE-anti IFN-γR and PE-anti IL-6R separately for 15 min followed by dialysis for 1 h. Then LMNP were analyzed by using a flow cytometer (CytoFlex S, Beckman Counter, California, USA).

4.5. Cytokine-sponging capability of LMNP

To investigate the cytokine sponge capability of different nanoparticles, LMNP (500 μg/ml) or its counterparts including MNP, NP, liposomes (Lip) and Vesicle were mixed with recombinant murine IFN-γ or IL-6 (500 pg/ml) at 37 °C for 30 min or 2 h in 1 ml of deionized water. Afterward, the mixture was spin down at 100,000×*g* for 30 min in a centrifuge and the IFN-γ or IL-6 concentration remained in the supernatant was determined by ELISA according to the routine protocols. To investigate the effect of medium on the cytokine sponge capability of LMNP, LMNP (500 μg/ml) was incubated with recombinant murine IFN-γ or IL-6 (500 pg/ml) in 1 ml of different mediums including deionized water, plasma, 10% FBS or PBS at 37 °C for 30 min. Afterward, the mixture was spin down and the IFN-γ or IL-6 concentration in the supernatant was determined as described above. To quantify the capacity of LMNP sponging cytokines, various concentrations of LMNP (0, 250, 500, 1000, 2000 μg/ml) were incubated with 500 pg/ml of recombinant murine IFN-γ or IL-6 in 1 ml of deionized water at 37 °C for 30 min. The mixture was spin down and the IFN-γ or IL-6 concentration in the supernatant was determined as described above. Furthermore, 500 μg/ml of LMNP was incubated with varied concentrations of recombinant murine IFN-γ (1000, 500, 250, 125, 0 pg/ml) or IL-6 (500, 250, 125, 25, 0 pg/ml) in 1 ml of deionized water at 37 °C for 30 min. Then the mixture was spin down and the IFN-γ or IL-6 concentration in the supernatant was determined as described above.

The serum samples of five patients diagnosed as HLH were collected and approved by the institutional review board of Huazhong University of Science and Technology. All HLH patients were diagnosed according to HLH-2004 diagnostic criteria. The serums of patients were tested for cytokine-sponging capability of LMNP *in vitro*. Briefly, LMNP (1 mg/ml) were mixed with the serum of HLH patient at 37 °C for 30 min. And then the mixture was spin down at 100,000×*g* for 30 min in a centrifuge and the IFN-γ or IL-6 concentration remained in the supernatant was determined by ELISA according to the routine protocols.

4.6. Extraction and culture of bone marrow-derived macrophages (BMDMs)

The extraction of BMDMs were performed as described previously [65]. BMDMs were isolated via flushing bone marrow from mouse femurs and tibias with sterile PBS, and then the suspension was filtered through a 40 μm Falcon cell strainer to discard large tissues, followed by erythrocyte lysis according to the standard procedure. After centrifugation at 600×*g* for 5 min at 4 °C, the collected cells were cultured in DMEM containing 10% FBS, 1% Penicillin-Streptomycin and 20 ng/ml of M-CSF to facilitate macrophage differentiation. Three days later, the

medium was replaced with fresh cell culture medium. On day 7, BMDMs were fully differentiated for further experiments.

4.7. Inhibiting IFN-γ or IL-6-induced BMDMs activation by LMNP in vitro

IFN-γ (100 or 1000 pg/ml) or IL-6 (100 or 2000 pg/ml) was pre-incubated with 1 mg/ml of LMNP for 30 min at room temperature. After centrifugation at 100,000×*g* for 30 min to remove nanoparticle pellet, the supernatant was collected for subsequent tests. To evaluate the effect of LMNP on macrophage activation induced by IFN-γ or IL-6, BMDMs were seeded into a 12-well plate at the density of 4×10^6 cells per well and incubated overnight. Afterward, BMDMs were incubated with DMEM containing 10% (v/v) supernatant or various concentrations of IFN-γ (100 and 1000 pg/ml) or IL-6 (100 and 2000 pg/ml) for 24 h. Then BMDMs were collected, resuspended in FACS buffer (PBS containing 2% FBS), incubated with APC-F4/80 and PE-CD80 for 20 min at 4 °C with gentle shaking, and subjected to flow cytometry analysis to identify the proportion of proinflammatory macrophages indicated by $F4/80^+CD80^+$. BMDMs without any treatment were used as a control group. BMDMs were fixed, permeated by Cytofix/Cytoperm Kit, stained with Percp/Cy5.5-pSTAT1 antibody or FITC-pSTAT3 antibody, washed once with PBS, and subjected to a flow cytometer to detect the intracellular expression levels of pSTAT1 and pSTAT3. RNA sequencing (RNA-seq) was adopted to explore the mechanism of inhibiting BMDMs activation by LMNP treatment. In brief, IFN-γ (100 ng/ml) was incubated with LMNP (1 mg/ml) for 30 min at room temperature, then the supernatant was collected. BMDMs were cultured and treated with DMEM containing 10% (v/v) supernatant or 10 ng/ml of IFN-γ for 24 h as described above. BMDMs treated with DMEM containing 10% (v/v) PBS served as control. Afterward, BMDMs were collected and total RNA was extracted from BMDMs using Trizol (Invitrogen, Carlsbad, CA, USA) according to the commercial instruction. Subsequently, total RNA was quantified using the Agilent 2100 bioanalyzer (Thermo Fisher Scientific, MA, USA) and passed quality control analysis on a Nano Drop (Thermo Fisher Scientific, MA, USA). Oligo(dT)-attached magnetic beads were utilized to purified mRNA. Purified mRNA was then subjected to reverse transcription for the purpose of cDNA synthesis. Next, obtained cDNA fragments were amplified by PCR, and products were purified by Ampure XP Beads, and validated on the Agilent Technologies 2100 bioanalyzer for quality control. The final library was prepared via circularizing the cDNA by the splint oligo sequence and was amplified with phi29 to make DNA nanoball (DNB) with more than 300 copies of one molecule. Finally, DNBs were loaded into the patterned nanoarray and sequenced as single end 50 bases reads on BGIseq500 platform (BGI-Shenzhen, China). The differentially expressed genes (DEGS) were screened according to Log_2 of fold-change and Q value ($|\log_2(\text{fold-change})| \geq 1$, Q value ≤ 0.05). Volcano map, Cluster analysis, Kyoto Encyclopedia of Genes and Genomes (KEGG) pathway analysis, and Key driver analysis (KDA) of the DEGS were conducted by Dr. Tom system (https://biosys.bgi.com).

4.8. Anti-HLH efficacy in the CpG-induced HLH model

CpG-induced mouse models of HLH were established as previously reported [45]. In brief, C57BL/6 J mice received intraperitoneal (i.p.) injection of CpG at a dose of 2 mg/kg per mouse every other day for five times. LMNP was administrated via the tail vein at a dose of 2 mg/kg per mouse every day (From Day 1 to Day 9). Mouse models receiving 100 μl of PBS served as a negative control and mouse models received α–IFN–γ injection at a dose of 5 mg/kg per mouse on Day 1, 3, 5, 7, 9 served as a positive control [44]. MNP and NP was administrated via the tail vein per mouse every day at a dose of 2 mg/kg (From Day 1 to Day 9) as controls.

At the end of the study, mouse models were sacrificed and blood was collected for inflammation cytokine analysis and blood routine test with the parameters including the count of red blood cell (RBC), white blood cell (WBC), platelet (Plt), hemoglobin (HgB) and hepatorenal function test with the parameters including triacylglycerol (TG), alanine transaminase (ALT), aspartate aminotransferase (AST) and blood urea nitrogen (BUN). Important organs including livers and spleens were obtained and weighed. The image of spleens was acquired, and thereafter the spleen tissues were smashed into single cell suspension and passed through a 40 μm cell strainer snap cap to remove large fibrous tissues. After centrifugation, RBCs in the precipitate were lysed with RBC lysis buffer. Then splenic cells were resuspended in FACS buffer (PBS containing 2% FBS), stained with Pacific Blue-CD45, APC-F4/80 and PE-CD80 for 20 min at 4 °C with gentle shaking, and subjected to flow cytometry to record the number of macrophages and the proportion of proinflammatory macrophages indicated by $CD45^+F4/80^+CD80^+$ cells. The intracellular expression of pSTAT1 and pSTAT3 in the macrophage was also evaluated by flow cytometry. Briefly, splenic cells were fixed, permeated by Cytofix/Cytoperm Kit (Biolegend), stained with PE-pSTAT1 antibody or FITC-pSTAT3 antibody, washed with PBS, and subjected to a flow cytometer. For hematophagocyte analysis, smears of spleen tissues from different treatment groups were prepared and Liu's stain was performed to detect hematophagocytes under a microscope (Olympus CKX53 Inverted Phase Contrast Fluorescence Microscope, Olympus, Japan). With regard to immunohistochemistry (IHC) staining of IFN-γ and IL-6, livers and spleens from different treatment groups were fixed in 4% paraformaldehyde overnight, rinsed in PBS, dehydrated, embedded in paraffin, and sectioned into slices of 8-μm thickness. Then the slices were subjected to IHC staining of IFN-γ and IL-6 according to commercial instructions.

4.9. Anti-HLH efficacy in the lethal HLH model

To establish the lethal HLH model, mice received an intravenous (i.v.) injection of 10 mg/kg of poly I:C and an i.p. administration of 5 mg/kg of LPS 24 h later. Afterward, LMNP was i.v. injected to the diseased mice at a dose of 8 mg/kg every 2 h for 2 or 4 times after LPS administration. α–IFN–γ was also given to the diseased mice at a dose of 10 mg/kg every 2 h for once or 4 times as positive controls. Equal volume of PBS was i.v. injected to the diseased mice every 2 h as a negative control. MNP and NP was administered intravenously to mice at a dose of 8 mg/kg every 2 h for 4 times after LPS administration. Mouse survival was recorded to plot the survival curve. Before the second treatment, blood samples were collected to measure the expression levels of IL-6, IL-10, IL-1β, TNF-α and IFN-γ in the serum by ELISA according to the manufacturer's instructions. And plasma was tested for prothrombin time (PT), activated partial thromboplastin time (ATPP) and fibrinogen (FIB). For hematophagocyte analysis, 4 h post the last treatment, mouse models were sacrificed. Smears of spleen tissues from different treatment groups were prepared and Liu's stain was performed to detect hematophagocytes under Olympus CKX53 Inverted Phase Contrast Fluorescence Microscope as described above.

4.10. Safety evaluation of LMNP

Equal volume of PBS and LMNP (at a dose of 40 mg/kg per mouse) were administrated into normal mice through the tail vein, and their blood was collected from the retro-orbital vein for the blood routine test, hepatorenal function test and inflammation cytokine analysis. Then the mice were sacrificed and their major organs including hearts, livers, spleens, lungs and kidneys were collected and sectioned for H&E staining.

4.11. Statistical analysis

Data were analyzed with Graphpad Prism (version 8), and all data were presented with mean ± SD (standard deviation). Statistical comparisons were conducted with an unpaired Student's *t*-test between two groups and one-way ANOVA with *posttest* among multiple groups.

Survival curves were plotted by using the Kaplan-Meier method.

Ethics approval and consent to participate

This study involving human blood sample was approved by the Ethics Committee of Union Hospital, Tongji Medical College, Huazhong University of Science and Technology. (2021.0818).

All mice were raised in the Center for Experimental Animals at School of Pharmacy, Fudan University. The animal experimental protocol was approved by the Animal Ethics Committee of Fudan University in compliance with national and institutional guidelines. (2017-03-YJ-PZQ-01).

CRediT authorship contribution statement

Honglan Wang: Conceptualization, Methodology, Writing – original draft. **Huiwen Liu:** Methodology, Writing – original draft. **Jia Li:** Investigation, Writing – review & editing. **Chunying Liu:** Investigation. **Hui Chen:** Investigation. **Junying Li:** Methodology. **Chunyan Sun:** Resources. **Tao Guo:** Resources. **Zhiqing Pang:** Writing – review & editing, Funding acquisition, Supervision. **Bo Zhang:** Conceptualization, Writing – review & editing, Funding acquisition. **Yu Hu:** Funding acquisition, Supervision.

Declaration of competing interest

The authors declare no conflict of interest.

Acknowledgements

We acknowledge the financial support from National Natural Science Foundation of China (82070228, 81773283) and the National Key R&D Program of China (No. 2019YFC1316204). We would like to thank the National Center for Protein Science Shanghai for our Cryo-EM analysis of LMNP structures.

Appendix A. Supplementary data

Supplementary data to this article can be found online at https://doi.org/10.1016/j.bioactmat.2022.09.012.

References

[1] A. Setiadi, et al., Malignancy-associated haemophagocytic lymphohistiocytosis, Lancet Haematol 9 (3) (2022) e217–e227.
[2] G. Griffin, S. Shenoi, G.C. Hughes, Hemophagocytic lymphohistiocytosis: an update on pathogenesis, diagnosis, and therapy, Best Pract. Res. Clin. Rheumatol. 34 (4) (2020), 101515.
[3] E.J. Vick, et al., Proliferation through activation: hemophagocytic lymphohistiocytosis in hematologic malignancy, Blood Adv 1 (12) (2017) 779–791.
[4] H. Al-Samkari, N. Berliner, Hemophagocytic lymphohistiocytosis, Annu. Rev. Pathol. 13 (2018) 27–49.
[5] S.L. Yang, et al., Associations between inflammatory cytokines and organ damage in pediatric patients with hemophagocytic lymphohistiocytosis, Cytokine 85 (2016) 14–17.
[6] M. Lu, et al., Clinical analysis and a novel risk predictive nomogram for 155 adult patients with hemophagocytic lymphohistiocytosis, Ann. Hematol. 100 (9) (2021) 2181–2193.
[7] H. Trottestam, et al., Chemoimmunotherapy for hemophagocytic lymphohistiocytosis: long-term results of the HLH-94 treatment protocol, Blood 118 (17) (2011) 4577–4584.
[8] J.I. Henter, et al., Treatment of hemophagocytic lymphohistiocytosis with HLH-94 immunochemotherapy and bone marrow transplantation, Blood 100 (7) (2002) 2367–2373.
[9] W. Zhang, et al., Etoposide, an anticancer drug involved in therapy-related secondary leukemia: enzymes at play, Transl Oncol 14 (10) (2021), 101169.
[10] M. Vallurupalli, N. Berliner, Emapalumab for the treatment of relapsed/refractory hemophagocytic lymphohistiocytosis, Blood 134 (21) (2019) 1783–1786.
[11] D.C. Fajgenbaum, C.H. June, Storm Cytokine, N. Engl. J. Med. 383 (23) (2020) 2255–2273.
[12] F. Locatelli, et al., Emapalumab in children with primary hemophagocytic lymphohistiocytosis, N. Engl. J. Med. 382 (19) (2020) 1811–1822.
[13] R. Das, et al., Janus kinase inhibition lessens inflammation and ameliorates disease in murine models of hemophagocytic lymphohistiocytosis, Blood 127 (13) (2016) 1666–1675.
[14] H. Wang, et al., Low dose ruxolitinib plus HLH-94 protocol: a potential choice for secondary HLH, Semin. Hematol. 57 (1) (2020) 26–30.
[15] A. Ahmed, et al., Ruxolitinib in adult patients with secondary haemophagocytic lymphohistiocytosis: an open-label, single-centre, pilot trial, Lancet Haematol 6 (12) (2019) e630–e637.
[16] A. Wei, et al., Short-term effectiveness of ruxolitinib in the treatment of recurrent or refractory hemophagocytic lymphohistiocytosis in children, Int. J. Hematol. 112 (4) (2020) 568–576.
[17] J. Wang, et al., Ruxolitinib for refractory/relapsed hemophagocytic lymphohistiocytosis, Haematologica 105 (5) (2020) e210–e212.
[18] N. Polverelli, et al., Second primary malignancy in myelofibrosis patients treated with ruxolitinib, Br. J. Haematol. 193 (2) (2021) 356–368.
[19] E. Porpaczy, et al., Aggressive B-cell lymphomas in patients with myelofibrosis receiving JAK1/2 inhibitor therapy, Blood 132 (7) (2018) 694–706.
[20] K. Jin, et al., Biomimetic nanoparticles for inflammation targeting, Acta Pharm. Sin. B 8 (1) (2018) 23–33.
[21] R. Li, et al., Route to rheumatoid arthritis by macrophage-derived microvesicle-coated nanoparticles, Nano Lett. 19 (1) (2019) 124–134.
[22] R. Liu, et al., Macrophage-mimic shape changeable nanomedicine retained in tumor for multimodal therapy of breast cancer, J. Contr. Release 321 (2020) 589–601.
[23] C. Hu, et al., Phagocyte-membrane-coated and laser-responsive nanoparticles control primary and metastatic cancer by inducing anti-tumor immunity, Biomaterials 255 (2020), 120159.
[24] C.M. Hu, et al., Erythrocyte membrane-camouflaged polymeric nanoparticles as a biomimetic delivery platform, Proc. Natl. Acad. Sci. U. S. A. 108 (27) (2011) 10980–10985.
[25] Y. He, et al., Erythroliposomes: integrated hybrid nanovesicles composed of erythrocyte membranes and artificial lipid membranes for pore-forming toxin clearance, ACS Nano 13 (4) (2019) 4148–4159.
[26] Z. Pang, et al., Detoxification of organophosphate poisoning using nanoparticle bioscavengers, ACS Nano 9 (6) (2015) 6450–6458.
[27] J.A. Copp, et al., Clearance of pathological antibodies using biomimetic nanoparticles, Proc. Natl. Acad. Sci. U. S. A. 111 (37) (2014) 13481–13486.
[28] Q. Zhang, et al., Neutrophil membrane-coated nanoparticles inhibit synovial inflammation and alleviate joint damage in inflammatory arthritis, Nat. Nanotechnol. 13 (12) (2018) 1182–1190.
[29] S. Thamphiwatana, et al., Macrophage-like nanoparticles concurrently absorbing endotoxins and proinflammatory cytokines for sepsis management, Proc. Natl. Acad. Sci. U. S. A. 114 (43) (2017) 11488–11493.
[30] M. Liu, B. López de Juan Abad, K. Cheng, Cardiac fibrosis: myofibroblast-mediated pathological regulation and drug delivery strategies, Adv. Drug Deliv. Rev. 173 (2021) 504–519.
[31] G. Prencipe, et al., Neutralization of IFN-γ reverts clinical and laboratory features in a mouse model of macrophage activation syndrome, J. Allergy Clin. Immunol. 141 (4) (2018) 1439–1449.
[32] P. Sackstein, J. Zaemes, C. Kim, Pembrolizumab-induced cytokine release syndrome in a patient with metastatic lung adenocarcinoma: a case report, J Immunother Cancer 9 (7) (2021).
[33] J.H. Park, et al., Genetically engineered cell membrane-coated nanoparticles for targeted delivery of dexamethasone to inflamed lungs, Sci. Adv. 7 (25) (2021).
[34] Y. Jiang, et al., Engineered cell-membrane-coated nanoparticles directly present tumor antigens to promote anticancer immunity, Adv Mater 32 (30) (2020) e2001808.
[35] G.Y. Xu, et al., Solution structure of recombinant human interleukin-6, J. Mol. Biol. 268 (2) (1997) 468–481.
[36] V. Veverka, et al., Conservation of functional sites on interleukin-6 and implications for evolution of signaling complex assembly and therapeutic intervention, J. Biol. Chem. 287 (47) (2012) 40043–40050.
[37] P.W. Gray, D.V. Goeddel, Cloning and expression of murine immune interferon cDNA, Proc. Natl. Acad. Sci. U. S. A. 80 (19) (1983) 5842–5846.
[38] Q. Ma, et al., Calming cytokine storm in pneumonia by targeted delivery of TPCA-1 using platelet-derived extracellular vesicles, Matter 3 (1) (2020) 287–301.
[39] X. Dai, et al., Targeting CAMKII to reprogram tumor-associated macrophages and inhibit tumor cells for cancer immunotherapy with an injectable hybrid peptide hydrogel, Theranostics 10 (7) (2020) 3049–3063.
[40] P.K. Langston, M. Shibata, T. Horng, Metabolism supports macrophage activation, Front. Immunol. 8 (2017) 61.
[41] A. Viola, et al., The metabolic signature of macrophage responses, Front. Immunol. 10 (2019) 1462.
[42] Q. Zhang, et al., A pilot study of ruxolitinib as a front-line therapy for 12 children with secondary hemophagocytic lymphohistiocytosis, Haematologica 106 (7) (2021) 1892–1901.
[43] M.B. Jordan, et al., An animal model of hemophagocytic lymphohistiocytosis (HLH): CD8+ T cells and interferon gamma are essential for the disorder, Blood 104 (3) (2004) 735–743.
[44] S. Albeituni, et al., Mechanisms of action of ruxolitinib in murine models of hemophagocytic lymphohistiocytosis, Blood 134 (2) (2019) 147–159.
[45] E.M. Behrens, et al., Repeated TLR9 stimulation results in macrophage activation syndrome-like disease in mice, J. Clin. Invest. 121 (6) (2011) 2264–2277.
[46] I. Tsuboi, et al., Senescence-accelerated mice (SAMP1/TA-1) treated repeatedly with lipopolysaccharide develop a condition that resembles hemophagocytic lymphohistiocytosis, Haematologica 104 (10) (2019) 1995–2005.

[47] A. Wang, et al., Specific sequences of infectious challenge lead to secondary hemophagocytic lymphohistiocytosis-like disease in mice, Proc. Natl. Acad. Sci. U. S. A. 116 (6) (2019) 2200–2209.
[48] E. Brisse, C.H. Wouters, P. Matthys, Hemophagocytic lymphohistiocytosis (HLH): a heterogeneous spectrum of cytokine-driven immune disorders, Cytokine Growth Factor Rev. 26 (3) (2015) 263–280.
[49] R. Karki, et al., Synergism of TNF-α and IFN-γ triggers inflammatory cell death, tissue damage, and mortality in SARS-CoV-2 infection and cytokine shock syndromes, Cell 184 (1) (2021) 149–168.e17.
[50] M. Hu, et al., Hepatic macrophages act as a central hub for relaxin-mediated alleviation of liver fibrosis, Nat. Nanotechnol. 16 (4) (2021) 466–477.
[51] B. Zhang, et al., Enhanced antitumor activity of EGFP-EGF1-conjugated nanoparticles by a multitargeting strategy, ACS Appl. Mater. Interfaces 8 (14) (2016) 8918–8927.
[52] B. Zhang, et al., Cyclopamine treatment disrupts extracellular matrix and alleviates solid stress to improve nanomedicine delivery for pancreatic cancer, J. Drug Target. 26 (10) (2018) 913–919.
[53] S. Li, et al., Pseudoneutrophil cytokine sponges disrupt myeloid expansion and tumor trafficking to improve cancer immunotherapy, Nano Lett. 20 (1) (2020) 242–251.
[54] Y. Zhao, et al., Lactoferrin-mediated macrophage targeting delivery and patchouli alcohol-based therapeutic strategy for inflammatory bowel diseases, Acta Pharm. Sin. B 10 (10) (2020) 1966–1976.
[55] M. Liu, et al., Bispecific antibody inhalation therapy for redirecting stem cells from the lungs to repair heart injury, Adv. Sci. 8 (1) (2021), 2002127.
[56] V. Buatois, et al., Use of a mouse model to identify a blood biomarker for IFNγ activity in pediatric secondary hemophagocytic lymphohistiocytosis, Transl. Res. 180 (2017) 37–52.e2.
[57] A.S. Yousif, et al., The persistence of interleukin-6 is regulated by a blood buffer system derived from dendritic cells, Immunity 54 (2) (2021) 235–246, e5.
[58] L.Y.C. Chen, et al., Soluble interleukin-6 receptor in the COVID-19 cytokine storm syndrome, Cell Rep Med 2 (5) (2021), 100269.
[59] M. Ramos-Casals, et al., Adult haemophagocytic syndrome, Lancet 383 (9927) (2014) 1503–1516.
[60] L.Y.C. Chen, et al., Confronting the controversy: interleukin-6 and the COVID-19 cytokine storm syndrome, Eur. Respir. J. 56 (4) (2020).
[61] S.K. Pierson, et al., Plasma proteomics identifies a 'chemokine storm' in idiopathic multicentric Castleman disease, Am. J. Hematol. 93 (7) (2018) 902–912.
[62] S.W. Canna, R.Q. Cron, Highways to hell: mechanism-based management of cytokine storm syndromes, J. Allergy Clin. Immunol. 146 (5) (2020) 949–959.
[63] C. Zhang, et al., Radiotherapy and cytokine storm: risk and mechanism, Front. Oncol. 11 (2021), 670464.
[64] G. Suntharalingam, et al., Cytokine storm in a phase 1 trial of the anti-CD28 monoclonal antibody TGN1412, N. Engl. J. Med. 355 (10) (2006) 1018–1028.
[65] A. Kadl, E. Galkina, N. Leitinger, Induction of CCR2-dependent macrophage accumulation by oxidized phospholipids in the air-pouch model of inflammation, Arthritis Rheum. 60 (5) (2009) 1362–1371.